Role of glycosylation in neuromuscular disorders (MVIMIG 747, May 17 2012)

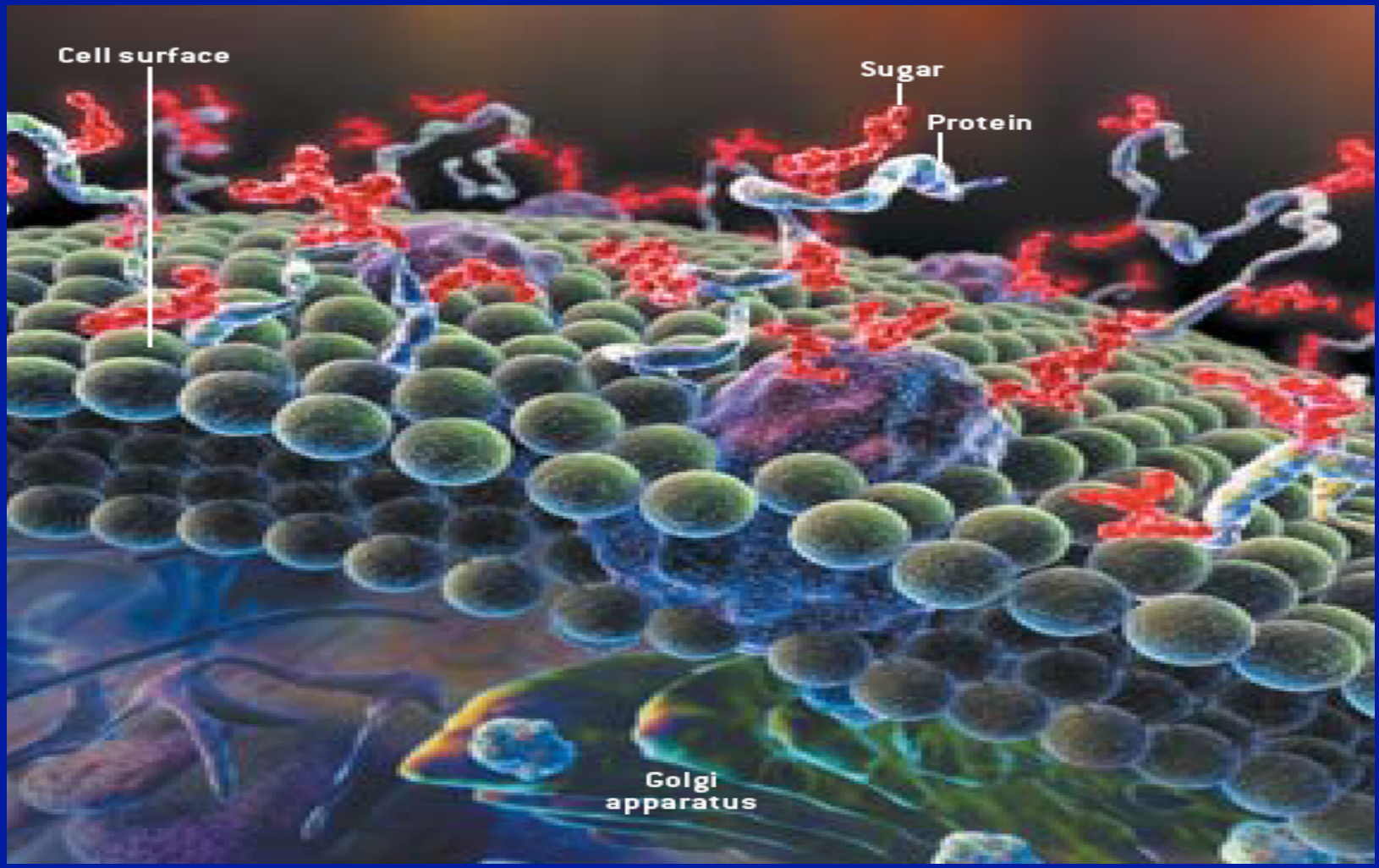

The glycocalyx

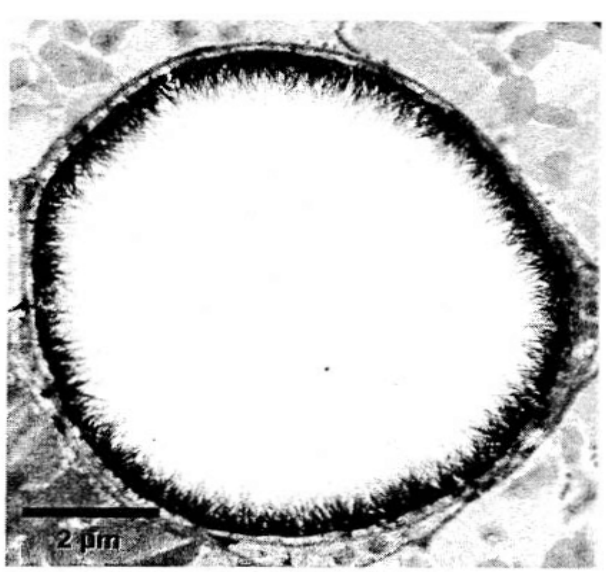

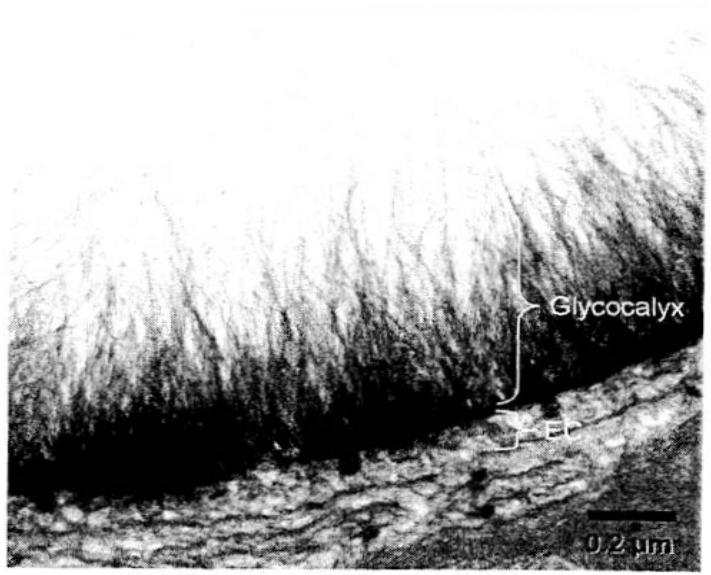

Fig. 1. Electron micrograph of a goat coronary capillary stained with Alcian blue

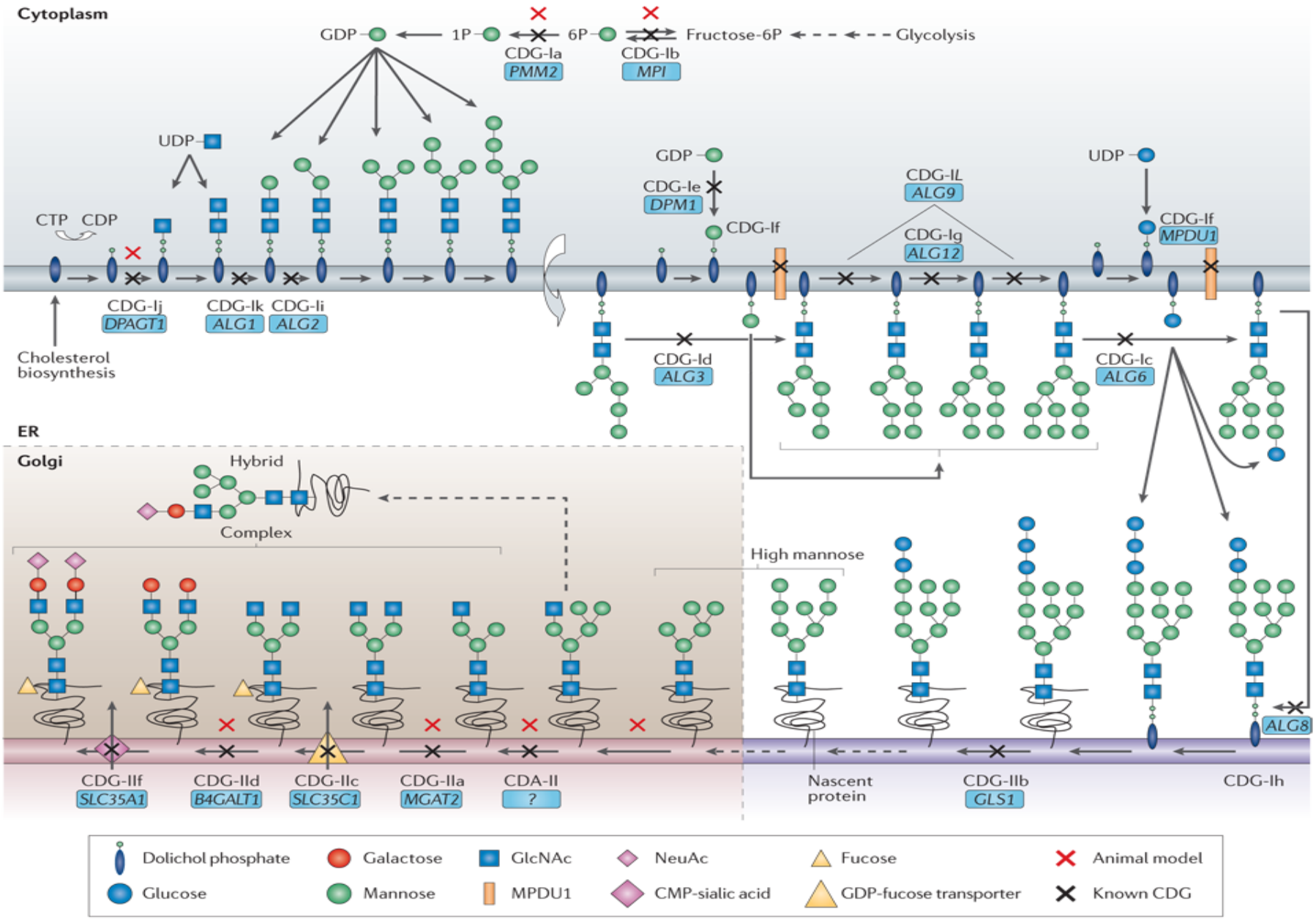

Figure 3 | **Sites of genetic defects in the *N*-linked glycan biosynthetic pathway.** During *N*-linked glycan biosynthesis, monosaccharides of GlcNAc (*N*-acetylglucosamine) and mannose are activated or interconverted and used

Table 2 | **Human diseases caused by genetic defects in *N*-glycosylation pathways**

Disorder	Gene	Enzyme	OMIM	Key Features
CDG-Ia	*PMM2*	Phosphomannomutase II	212065	Mental retardation, hypotonia, esotropia, lipodystrophy, cerebellar hypoplasia, stroke-like episodes, seizures
CDG-Ib	*MPI*	Phosphomannose isomerase	602579	Hepatic fibrosis, protein-losing enteropathy, coagulopathy, hypoglycaemia
CDG-Ic	*ALG6*	Glucosyltransferase I Dol-P-Glc: Man_9-$GlcNAc_2$-P-P-Dol glucosyltransferase	603147	Moderate mental retardation, hypotonia, esotropia, epilepsy
CDG-Id	*ALG3*	Dol-P-Man:Man_5-$GlcNAc_2$-P-P-Dol mannosyltransferase	601110	Profound psychomotor delay, optic atrophy, acquired microcephaly, iris colobomas, hypsarrhythmia
CDG-Ie	*DPM1*	Dol-P-Man synthase I GDP-Man: Dol-P-mannosyltransferase	603503	Severe mental retardation, epilepsy, hypotonia, mild dysmorphism, coagulopathy
CDG-If	*MPDU1*	Man-P-Dol utilization 1/Lec35	608799	Short stature, icthyosis, psychomotor retardation, pigmentary retinopathy
CDG-Ig	*ALG12*	Dol-P-Man:Man_7-$GlcNAc_2$P-P-Dol mannosyltransferase	607143	Hypotonia, facial dysmorphism, psychomotor retardation, acquired microcephaly, frequent infections
CDG-Ih	*ALG8*	Glucosyltransferase II Dol-P-Glc: Glc_1-Man_9-$GlcNAc_2$-P-P-Dol glucosyltransferase	608104	Hepatomegaly, protein-losing enteropathy, renal failure, hypoalbuminaemia, oedema, ascites
CDG-Ii	*ALG2*	Mannosyltransferase II GDP-Man: Man_1-$GlcNAc_2$-P-P-Dol mannosyltransferase	607906	Normal at birth; mental retardation, hypomyelination, intractable seizures, iris colobomas, hepatomegaly, coagulopathy
CDG-Ij	*DPAGT1*	UDP-GlcNAc: Dol-P-GlcNAc-P transferase	608093	Severe mental retardation, hypotonia, seizures, microcephaly, exotropia
CDG-Ik	ALG1	Mannosyltransferase I GDP-Man: $GlcNAc_2$-P-P-Dol mannosyltransferase	608540	Severe psychomotor retardation, hypotonia, acquired microcephaly, intractable seizures, fever, coagulopathy, nephrotic syndrome, early death
CDG-Il	*ALG9*	Mannosyltransferase Dol-P-Man: Man_6- and Man_8-$GlcNAc_2$-P-P-Dol mannosyltransferase	608776	Severe microcephaly, hypotonia, seizures, hepatomegaly
CDG-IIa	*MGAT2*	GlcNAc transferase 2	212066	Mental retardation, dysmorphism, stereotypies, seizures
CDG-IIb	*GLS1*	Glucosidase I	606056	Dysmorphism, hypotonia, seizures, hepatomegaly, hepatic fibrosis; death at 2.5 months
CDG-IIc	*SLC35C1/ FUCT1*	GDP-fucose transporter	266265	Recurrent infections, persistent neutrophilia, mental retardation, microcephaly, hypotonia; normal transferrin
CDG-IId	*B4GALT1*	β1,4 galactosyltransferase	607091	Hypotonia (myopathy), spontaneous haemorrhage, Dandy–Walker malformation
CDG-IIe	*COG7*	Conserved oligomeric Golgi complex subunit 7	608779	Fatal in early infancy; dysmorphism, hypotonia, intractable seizures, hepatomegaly, progressive jaundice, recurrent infections, cardiac failure
CDG-IIf	*SLC35A1*	CMP-sialic acid transporter	605634	Thrombocytopaenia, no neurological symptoms; normal transferrin, abnormal platelet glycoproteins
CDG-II/COG1	COG1	Conserved oligomeric Golgi complex subunit 1	606973	Hypotonia, growth retardation, progressive microcephaly, hepatosplenomegaly, mild mental retardation
Mucolipidosis II and III	*GNPTA*	UDP-GlcNAc: lysosomal enzyme, GlcNAc-P transferase	252500	Coarsening features, organomegaly, joint stiffness, dysostosis, median neuropathy at the wrist; MLIII is less severe than MLII, which presents in infancy
Congenital dyserythropoietic anaemia (CDA II)	Unknown	Unknown	224100	Anaemia, jaundice, splenomegaly, gall bladder disease

CDG, congenital disorders of glycosylation; Dol-P-Glc, dolichol-phosphate-glucose; GlcNAc, *N*-acetylglucosamine; Man, mannose.

Table 3 | **Human diseases caused by genetic defects in *O*-glycosylation and glycolipid synthesis pathways**

Disorder	Gene	Enzyme	OMIM	Key Features
Defects in O-glycosylation pathways				
Walker–Warburg syndrome	*POMT1/ POMT2*	*O*-mannosyltransferase 1	236670	Type II lissencephaly, cerebellar malformations, ventriculomegaly, anterior chamber malformations, severe delay; death in infancy
Fukuyama muscular dystrophy	*FCMD*	Fukutin, a putative glycosyltransferase	253800	Cortical dysgenesis, myopia, weakness and hypotonia; 40% have seizures
Congenital muscular dystrophy type 1C (MDC1C)	*FKRP*	Fukutin-related protein, a putative glycosyltransferase	606612	Hypotonia, impaired motor development, respiratory muscle weakness
Congenital muscular dystrophy type 1D (MDC1D)	*LARGE*	Putative glycosyltransferase	608840	Muscular dystrophy with profound mental retardation
Hereditary inclusion-body myopathy-II (IBM2)	*GNE*	UDP-GlcNAc epimerase/kinase	600737	Adult onset with progressive distal and proximal muscle weakness; spares quadriceps
Ehlers–Danlos syndrome	*B4GALT7*	β1,4-Galactosyltransferase 7	130070	Progeroid Ehlers-Danlos syndrome; macrocephaly, joint hyperextensibility
Heriditary multiple exostosis	*EXT1/ EXT2*	Glucuronyltransferase/GlcNAc transferase	133700	Multiple exostoses (diaphyseal, juxtaepiphyseal)
Chondrodysplasias	*DTDST/ SLC26A2*	Sulphate anion transporter	222600 600972 256050	Diastrophic dysplasia: airway collapse, early death in severe cases, adults reported. Achondrogenesis Ib: usually stillborn or early death of respiratory failure. Atelosteogenesis II: pulmonary hypoplasia, fatal in infants
Spondylo-epimetaphyseal dysplasia	*ATPSK2*	3′-phosphoadenosine-5′-phosphosulphate synthase	603005	Abnormal skeletal development and linear growth
Macular corneal dystrophy types I and II	*CHST6*	Keratan sulphate 6-0-sulphotransferase	217800	Corneal clouding and erosions, painful photophobia
Familial tumoral calcinosis	*GALNT3*	GalNAc transferase	211900	Massive calcium deposits in skin and tissue
Tn syndrome	*COSMC*	Chaperone of β1,3GalT	230430	Anaemia, leukopaenia, thrombocytopaenia (somatic mutation)
Defects in glycolipid synthesis				
Paroxysmal nocturnal haemoglobinuria	*PIGA*	PI-GlcNAcT	311770	Complement-mediated haemolysis (somatic mutation)
Amish infantile epilepsy	*SIAT9*	Sia2,3Galβ1,4Glc-Cer synthase	609056	Tonic-clonic seizures, arrested development, neurological decline

Three related cases of muscular dystrophy

Case 1. Newborn, severely hypotonic, minimal brain function, blindness (retinal detachment), muscular dystrophy. Death prior to 1 year of age.

Case 2. Teenager, significant mental retardation, ambulatory until teens, myopia, cataracts, muscular dystrophy. Death in early twenties.

Case 3. 30 yr. old with muscle weakness and mild cardiomyopathy (no symptoms until 20s), normal neurological workup. Normal lifespan.

All are caused by a molecular defect in the glycosylation of dystroglycan.

Three related cases of muscular dystrophy

Case 1. Newborn, severely hypotonic, minimal brain function, blindness (retinal detachment), muscular dystrophy. Death prior to 1 year of age.

Walker-Warburg Syndrome

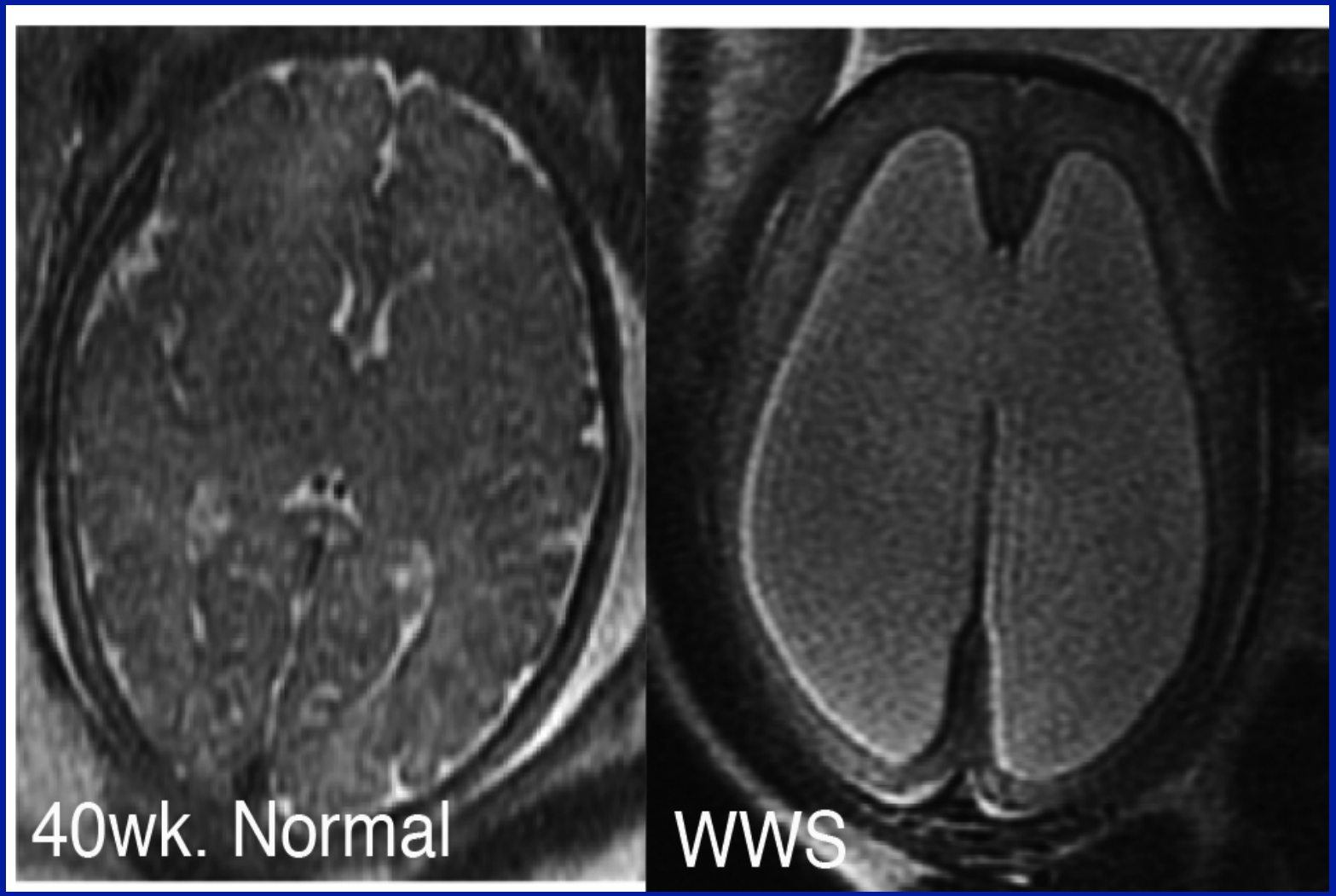
40wk. Normal
WWS

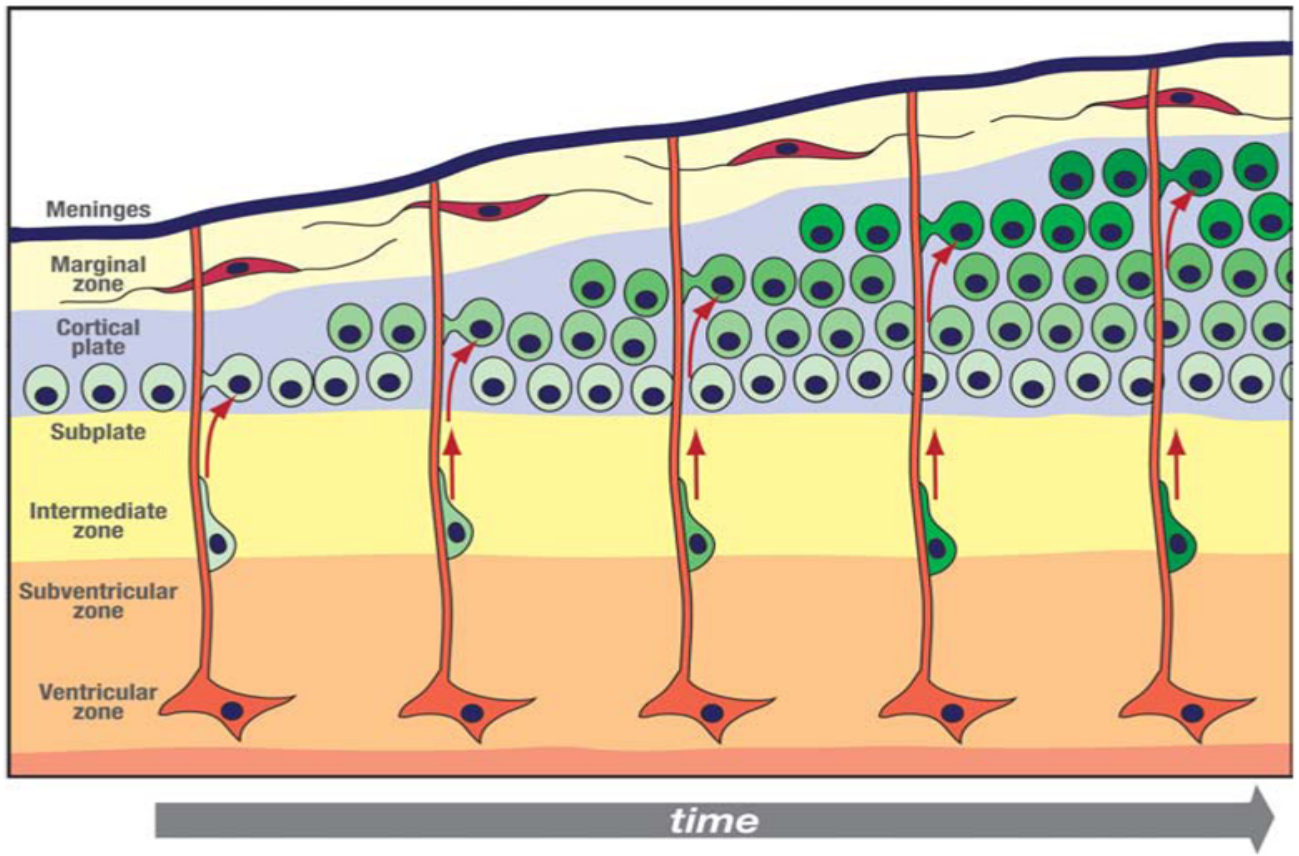

Figure 1 Schematic diagram of radial-directed cortical neuronal migration. Neurons (*green*) are generated in the ventricular zone and migrate along radial glial cells (*orange*) through the subventricular zone, intermediate zone, subplate, and cortical plate. The cortical plate is established in an inside-out pattern so that later-generated neurons (*progressively darker green shading*) destined for more superficial layers bypass earlier-generated neurons in deeper layers. The marginal zone includes horizontally oriented Cajal-Retzius (*red*). The most superficial cortical structure is the pia/meninges.

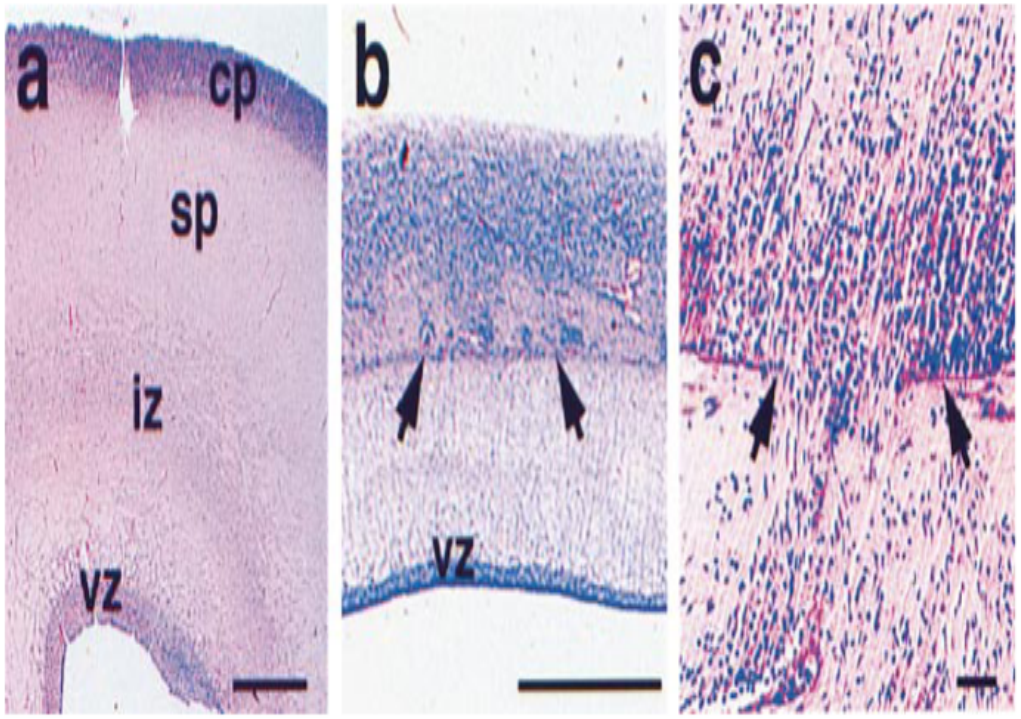

Figure 4. Cellular Appearance of Cobblestone (Type II) Lissencephaly

The photomicrographs contrast (a) a normal human fetal brain (22 weeks gestation) with the brain of a fetus of the same age with cobblestone lissencephaly due to Walker-Warburg syndrome (b and c). The brain in cobblestone lissencephaly (b) is less than half of normal thickness and lacks the clear stratification of the ventricular zone (vz), intermediate zone (iz), subplate (sp), and cortical plate (cp) seen in the normal brain (a). In both pictures, the ventricular surface is down and the pial surface is up. In (b), the location of the normal pial surface is indicated by arrows. The dark blue nuclei represent migrating cells that have penetrated the pia and flowed out randomly over the outer surface of the pia. The photomicrograph in (c) shows a higher power view of one of the defects in the pia, with immature neuroblasts migrating through it. Scale bar in (a) and (b), 1 mm; in (c), 100 μm.

Three related cases of muscular dystrophy

Case 2. Teenager, significant mental retardation, ambulatory until teens, myopia, cataracts, muscular dystrophy. Death in early twenties.

Muscle Eye Brain Disease

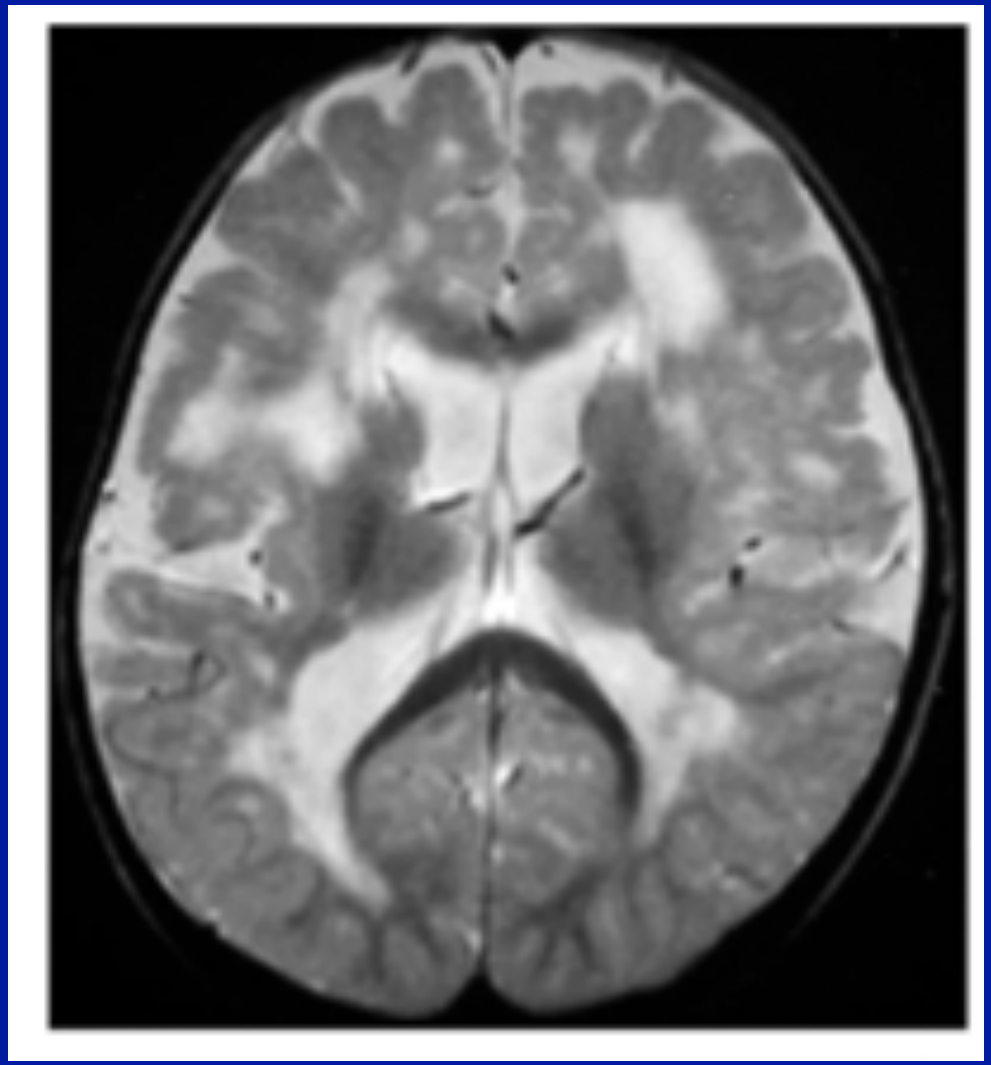

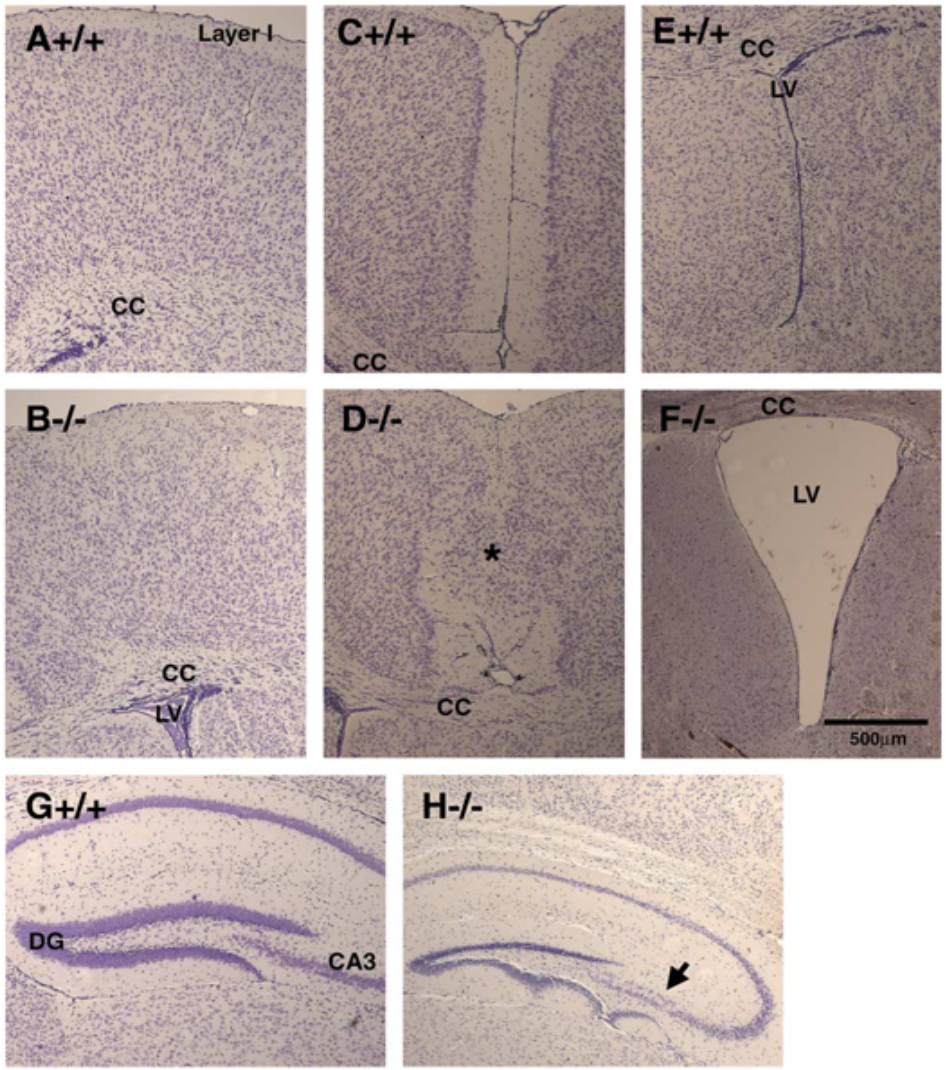

Fig. 6. Multiple abnormalities in the forebrain of POMGnT1 mutant mice. Paraffin sections of the forebrain were Nissle-stained (cresyl violet). (A) Wildtype cerebral cortex. (B) Mutant cerebral cortex. (C) Wildtype midline. (D) Mutant midline. (E) Wildtype lateral ventricle. (F) Mutant lateral ventricle. (G) Wildtype hippocampus. (H) Mutant hippocampus. Abbreviations: CC, caupus callosum; DG, dentate gyrus; LV, lateral ventricle. Scale bar in F, 500 μm.

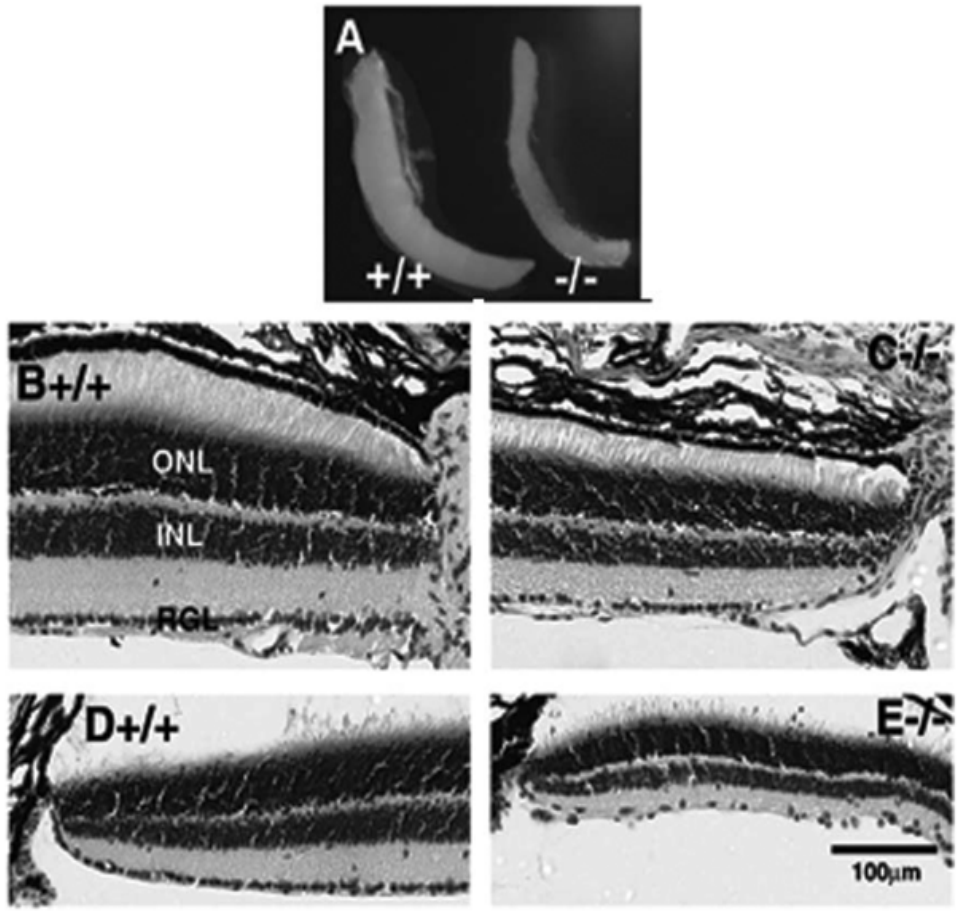

Fig. 7. Abnormal retina in POMGnT1 mutant mice. (A) Optic nerve of the mutant (−/−) and wildtype (+/+) mice. (B) Wildtype central retina. (C) Mutant central retina. (D) Wildtype peripheral retina. (E) Mutant peripheral retina. Note that the mutant retina has fewer ganglion cells especially in the peripheral retina. In addition, the retinal layers are thinner in the mutant. Abbreviations: INL, inner nuclear layer; ONL, outer nuclear layer; RGL, retinal ganglion cell layer. Scale bar in E, 100 μm for B–E.

Three related cases of muscular dystrophy

Case 3. 30 yr. old with muscle weakness and mild cardiomyopathy (no symptoms until 20s), normal neurological workup.

Limb Girdle Muscular dystrophy 2I


a

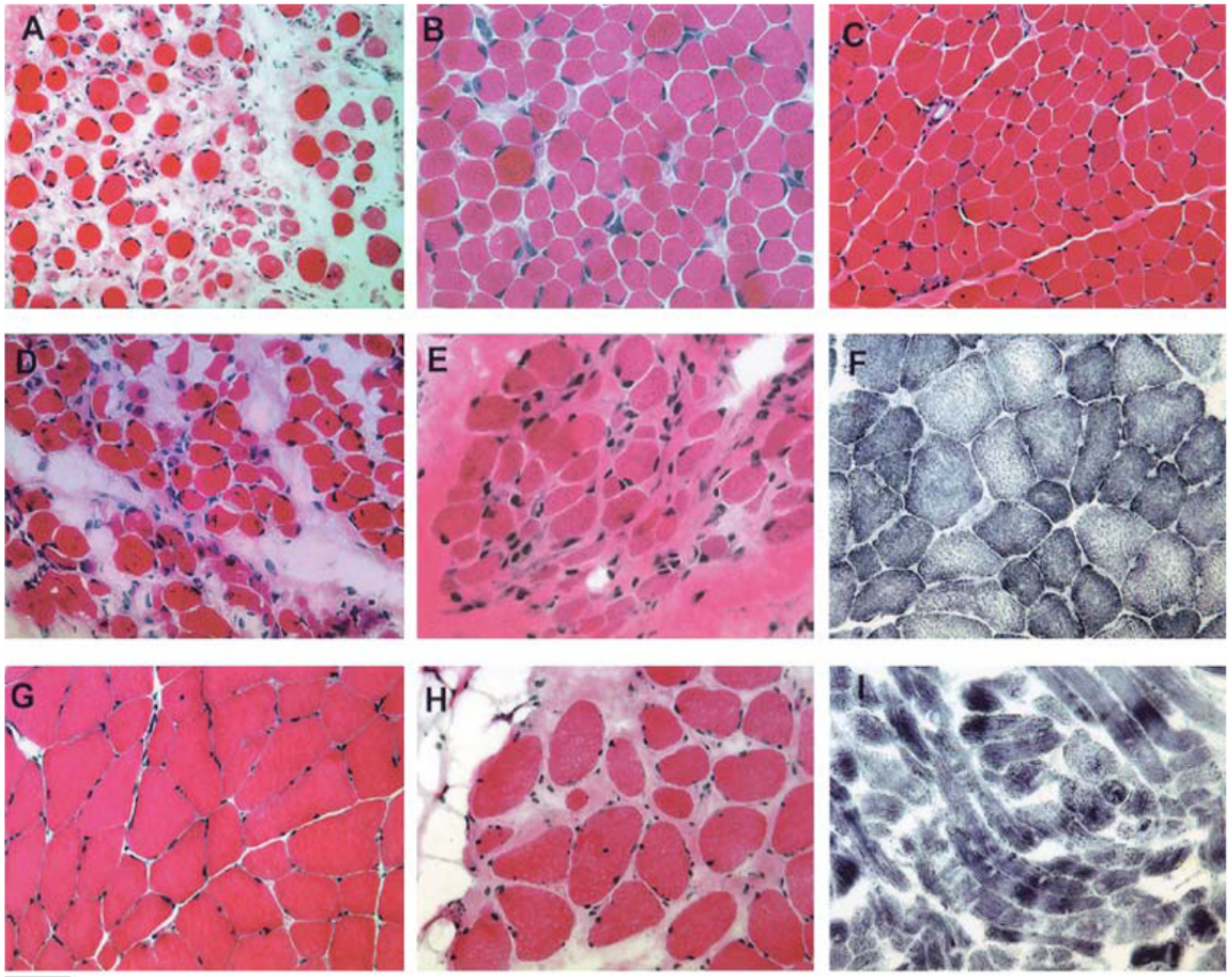

Figure 2. Muscle pathology of CMD. (*A*, *B*, *C*, *D*, *E*, *G* and *H*): Haematoxilin and eosin showing the variable degree of fibrosis, variation in muscle fibre diameter and degeneration. (*F* and *I*) Oxidative enzyme stain (NADH-TR). Type I fibres are more intensely stained because of their higher mitochondrial content. Pale areas reflect focal mitochondrial depletion and myofibrillar disruption in *F* and *I* (cut longitudinally). (*A*) MDC1C, (*B*) MEB, (*C*) MDC1D, (*D*) WWS, (*E*) MDC1A, (*F*, *G*) RSMD1, (*H* and *I*) UCMD. Scale bar represents 118 µm in *A*, *C*, *D*, *F*, *G*, *H*, *I* and 38 µm in *B* and *E*.

Dystroglycanopathies
Congenital and Limb Girdle Muscular Dystrophies

<u>Genes</u>
POMT1
POMT2
POMGnT1
Fukutin (*FCMD*)
Fukutin-related Protein (*FKRP*)
LARGE^{myd}

DPM2
DPM3
DAG1

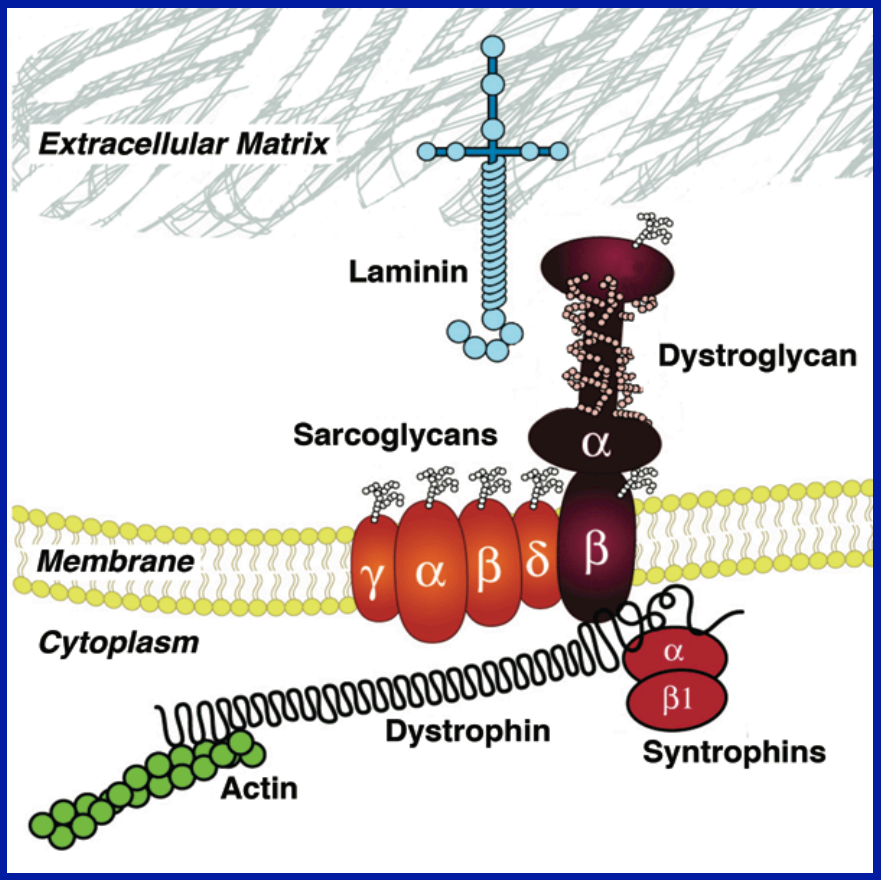

<u>Diseases</u>
WWS
MEB
FCMD
MCD1C
MCD1D
LGMD2I
LGMD2K
LGMD2L
LGMD2M
LGMD2N

Xylα1,3GlcAβ1,3
Neu5Ac/Gcα2,3Galβ1,4GlcNAcβ1,2Man(PO_4)α-O-Ser/Thr

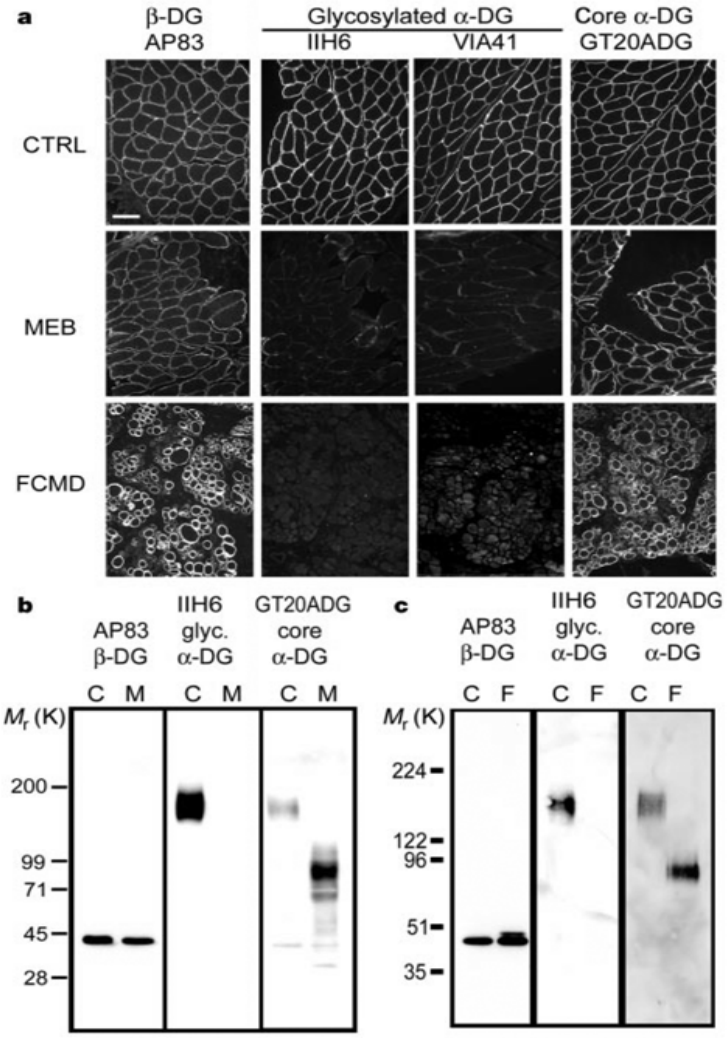

Figure 1 Post-translational modification of dystroglycan in MEB and FCMD. **a**, Immunofluorescence localization of dystroglycan in biopsies of normal muscle (CTRL) and muscle of MEB and FCMD patients, using antibodies against β-DG, glycosylated α-DG, and α-DG core protein. Data shown are representative of all four MEB and all three FCMD patients. Scale bar, 100 μm. **b**, **c**, Immunoblot analyses of age-matched normal (C) and MEB patient (M, **b**) and FCMD patient (F, **c**) WGA-enriched total muscle glycoproteins.

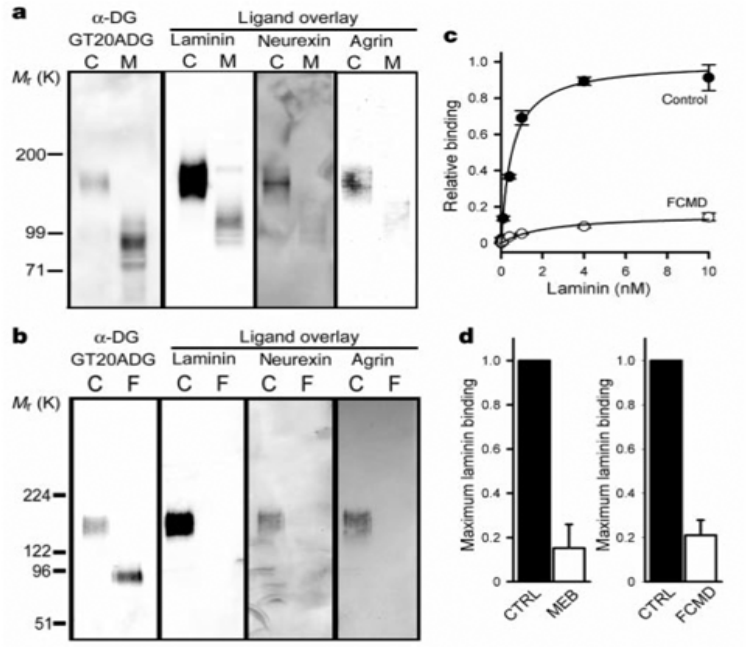

Figure 2 Dystroglycan–ligand interactions in MEB and FCMD. **a**, **b**, Ligand overlay assays on age-matched control (C) and MEB patient (M, **a**) and FCMD (F, **b**) WGA-enriched muscle homogenates using murine EHS laminin, neurexin fusion protein and recombinant rat agrin. **c**, Representative assay of solid-phase laminin-binding activity from control and FCMD muscle. Data are mean ± s.d. of triplicate samples fitted to a one-site model using the equation $A = B_{max}x/(K_d + x)$. **d**, Maximum laminin-binding activity in MEB ($n = 2$) and FCMD ($n = 3$) WGA glycoproteins relative to age-matched control muscle (CTRL). Data are mean ± s.e.m.

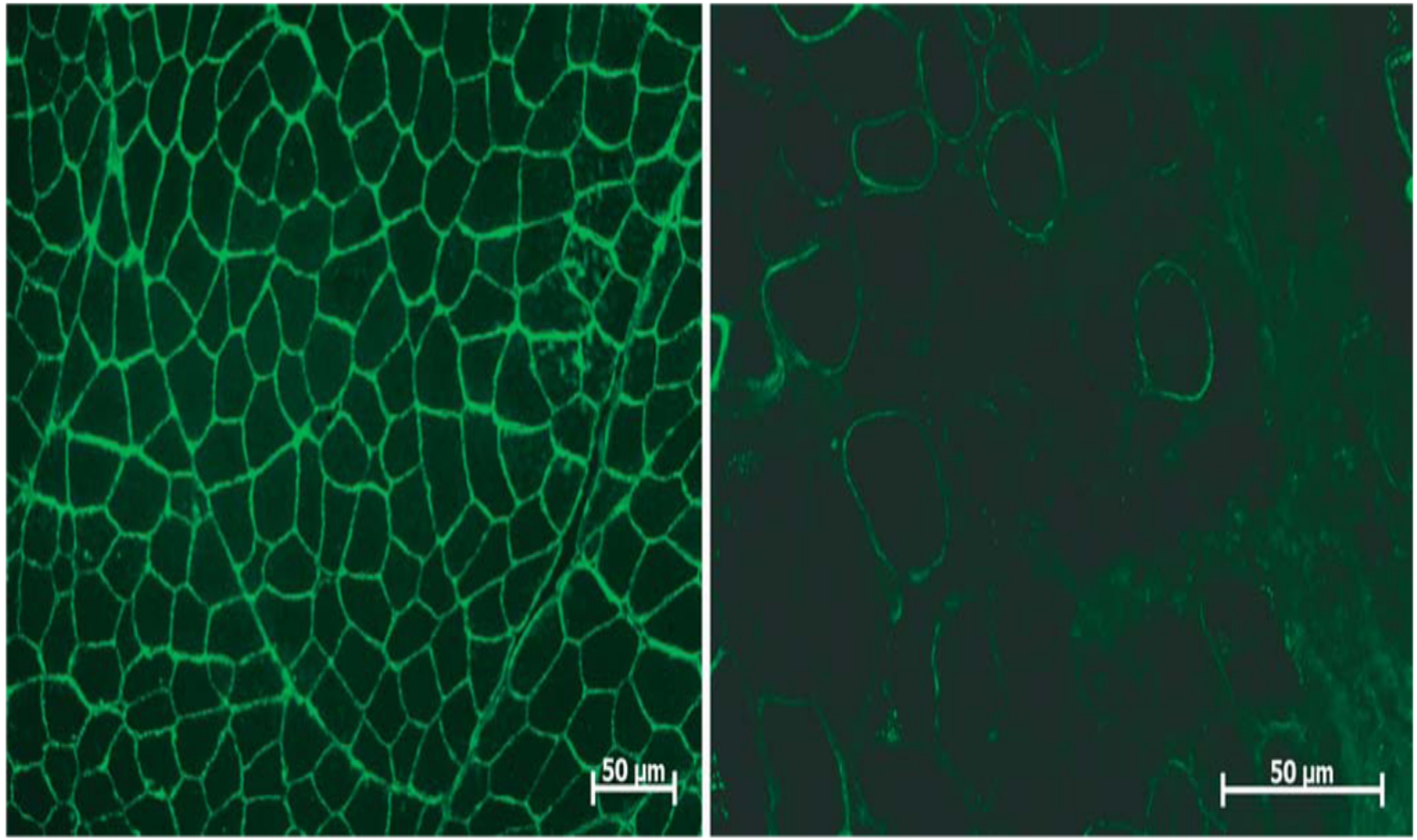

Figure 8. Stain for glycosylated α–dystroglycan (Upstate Cell Signaling Solutions, Lake Placid, NY, USA) in normal muscle compared with marked reduction in a patient with fukutin-related protein (FKRP) deficiency (MDC1C).

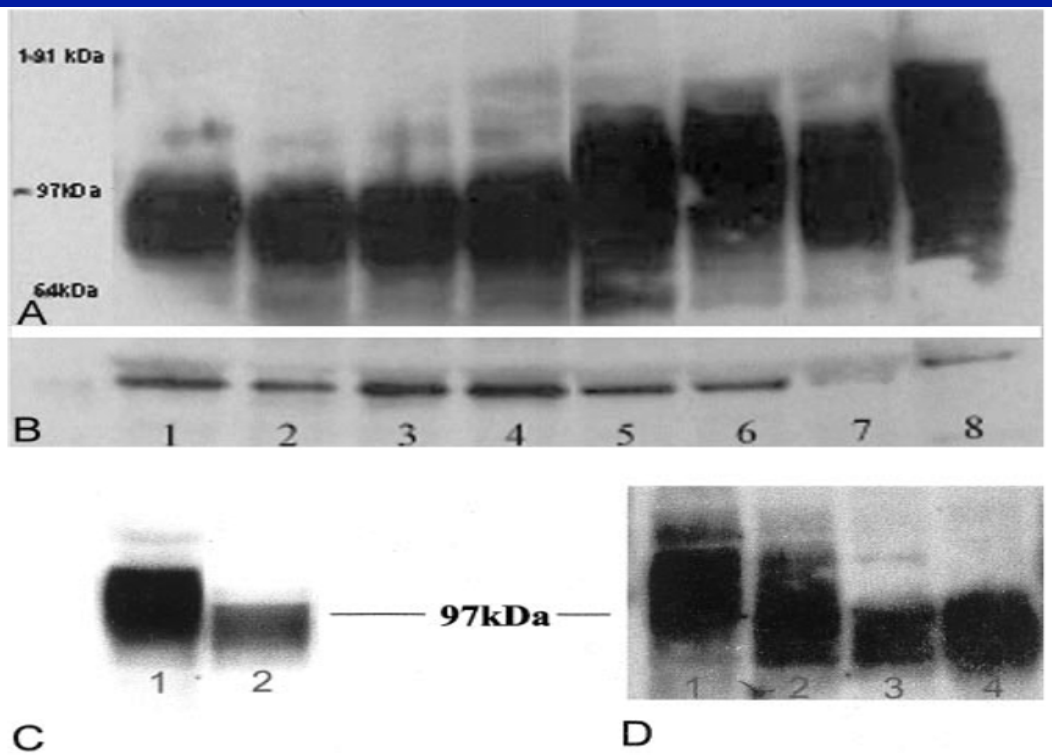

Figure 8. A: Western blot analysis of human fetal muscle at 9.4 weeks (**lane 1**), 10.9 weeks (**lane 2**), 13.6 weeks (**lane 3**), and 16.6 weeks (**lane 4**) of gestation, neonatal muscle (**lane 5**), adult muscle 9 (**lane 6**), DMD muscle (**lane 7**), and normal adult muscle (**lane 8**) are included for comparison. The average molecular weight of α-dystroglycan can be seen to increase with gestational age. **B:** Western blot shown in **A** probed for β-dystroglycan. **C:** Western blot analysis using V1A4–1 of muscle from control (**lane 1**) and LGMD2I (**lane 2**) at the severe end of the clinical spectrum. **D:** Western blot analysis using V1A4–1 of muscle from control (**lane 1**), LGMD2I homozygous for the Leu276Ile change (**lane 2**), MDC1C (**lane 3**), and human fetal muscle at 9.4 weeks gestation (**lane 4**).

Are CMD cellular defects dystroglycan-specific?

- Glycosyltransferases usually alter glycosylation of multiple substrate proteins and lipids
- In this instance, however, alpha dystroglycan is the only known recipient of these O-mannose structures
- Can phenocopy glycosylation defects by making DAG1-KO cells in vivo

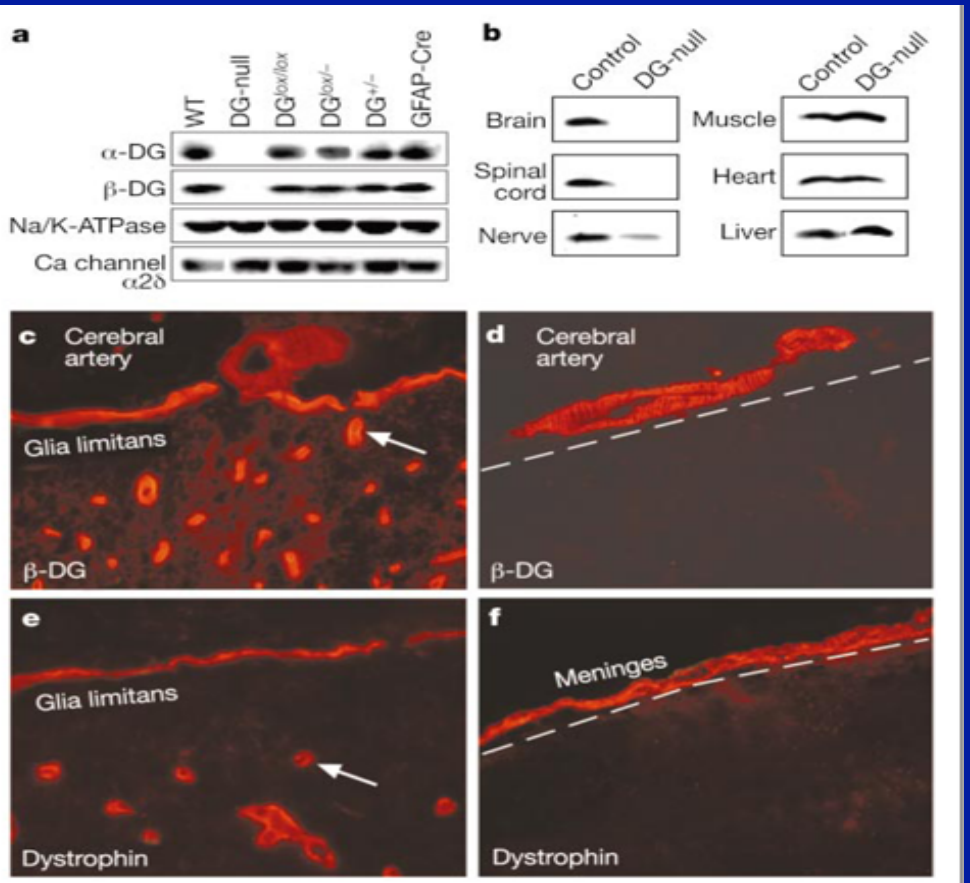

Figure 1 Tissue-selective deletion of dystroglycan. **a**, Western blot analysis of brain. WT, wild type; DG-null, GFAP-Cre/DG-null; $DG^{+/-}$, heterozygous dystroglycan null; $DG^{lox/-}$, heterozygous floxed/dystroglycan-null; $DG^{lox/lox}$, homozygous floxed. **b**, Western blot with a β-DG antibody. **c**, β-DG immunofluorescence of control cerebral cortex shows staining of smooth muscle in a small cerebral artery on the pial surface and astrocyte foot processes along the glia limitans and cerebral microvessels (arrow points to one microvessel). **d**, β-DG immunofluorescence is retained in only a small cerebral artery on the surface of DG-null cerebrum. **e**, Dystrophin immunofluorescence parallels that of β-DG in control brain. **f**, Dystrophin immunofluorescence is retained only in vessels of the meninges of DG-null brain. The position of the unstained glia limitans is marked by a dashed white line in **d** and **f**.

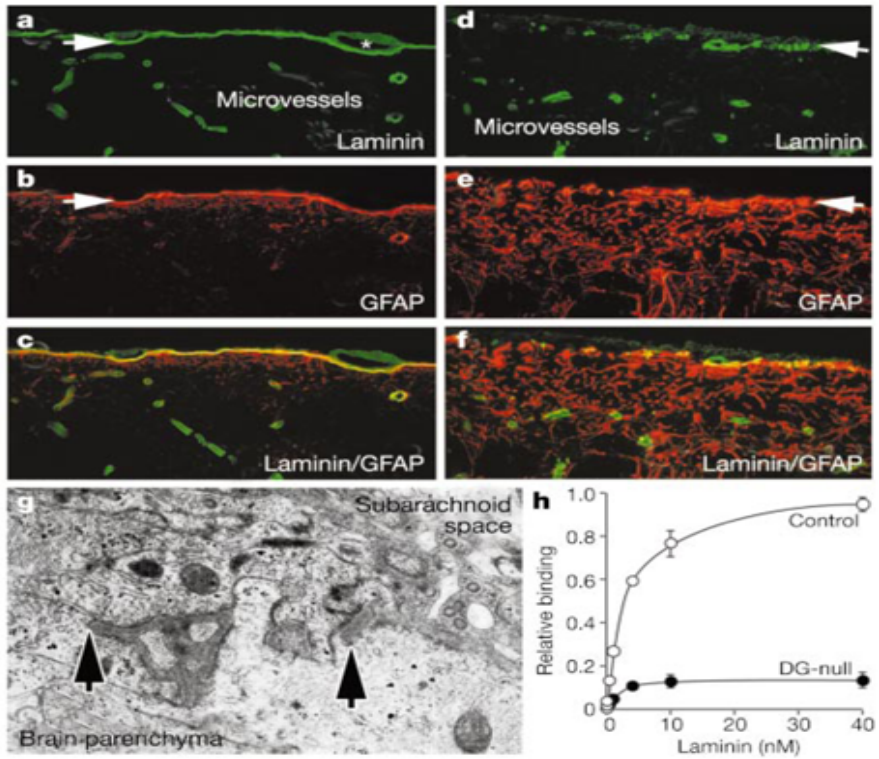

Figure 3 Disruptions of the glia limitans, leptomeningeal heterotopia and abnormal laminin binding. **a**, **d**, Laminin immunofluorescence (green) is present in the leptomeninges, pial vessels (asterisk in **a**), glia limitans (white arrows), and intracerebral microvessels of both control (**a**) and DG-null mice (**d**). The glia limitans is disrupted in DG-null mice (**d**). **b**, **e**, GFAP immunofluorescence (red) is prominent in only a superficial layer of astrocytes in control mice (**b**), but extends throughout the cortex in DG-null mice (**e**) (white arrows indicate glia limitans). **c**, **f**, Superimposing these images shows immunofluorescent overlap (yellow) between laminin and GFAP-stained astrocytic foot processes at the glia limitans and surrounding intracerebral blood vessels. Astrocytic processes extend through gaps in the glia limitans to form leptomeningeal heterotopia in DG-null mice (**f**). **g**, Electron microscopy confirms interruptions in the basal lamina of the glia limitans in DG-null mice (arrows), which should form a continuous horizontal band across the middle of this micrograph. Instead of being open, the subarachnoid space (upper portion of micrograph) is filled with cell processes. **h**, Total laminin binding is plotted for DG-null and littermate control brains. Binding in the absence of calcium was subtracted before plotting these curves.

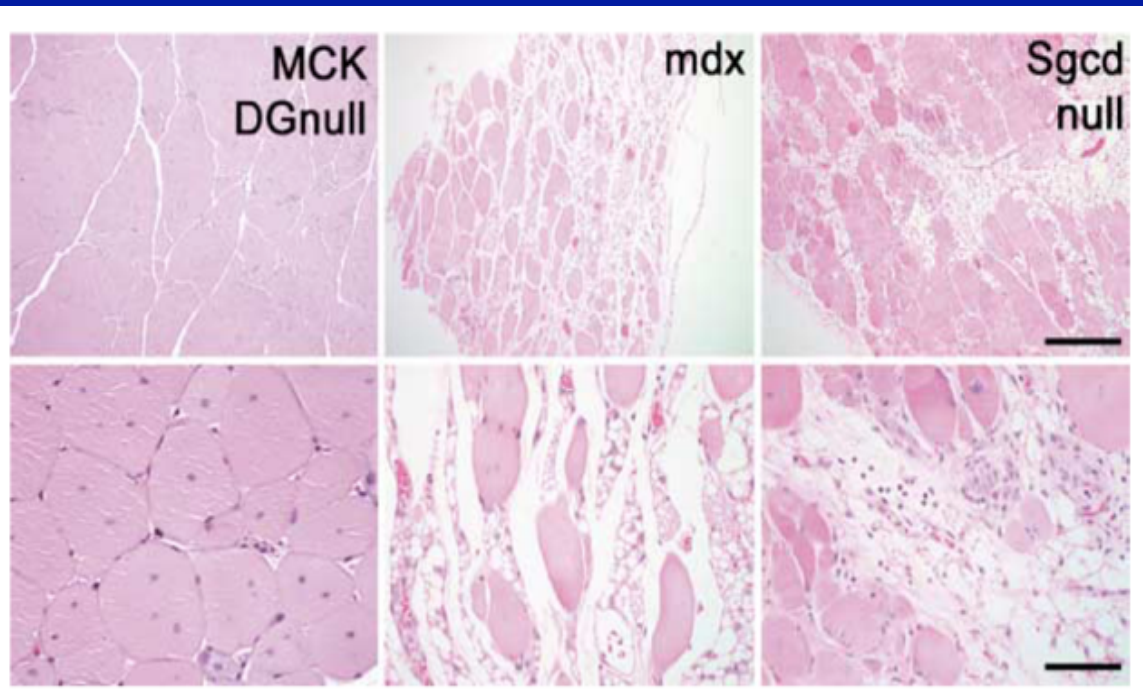

Figure 6. Comparison of Muscular Dystrophy in 18-Month-Old Mice

The capability of *MCK-DG null* mice to efficiently maintain skeletal muscle regeneration not only leads to significant muscle hypertrophy, but also prevents the development of severe dystrophic alterations as observed in mdx and *Sgcd null* mice. Bars represent 50 μm and 120 μm, in the upper and lower right panels, respectively.

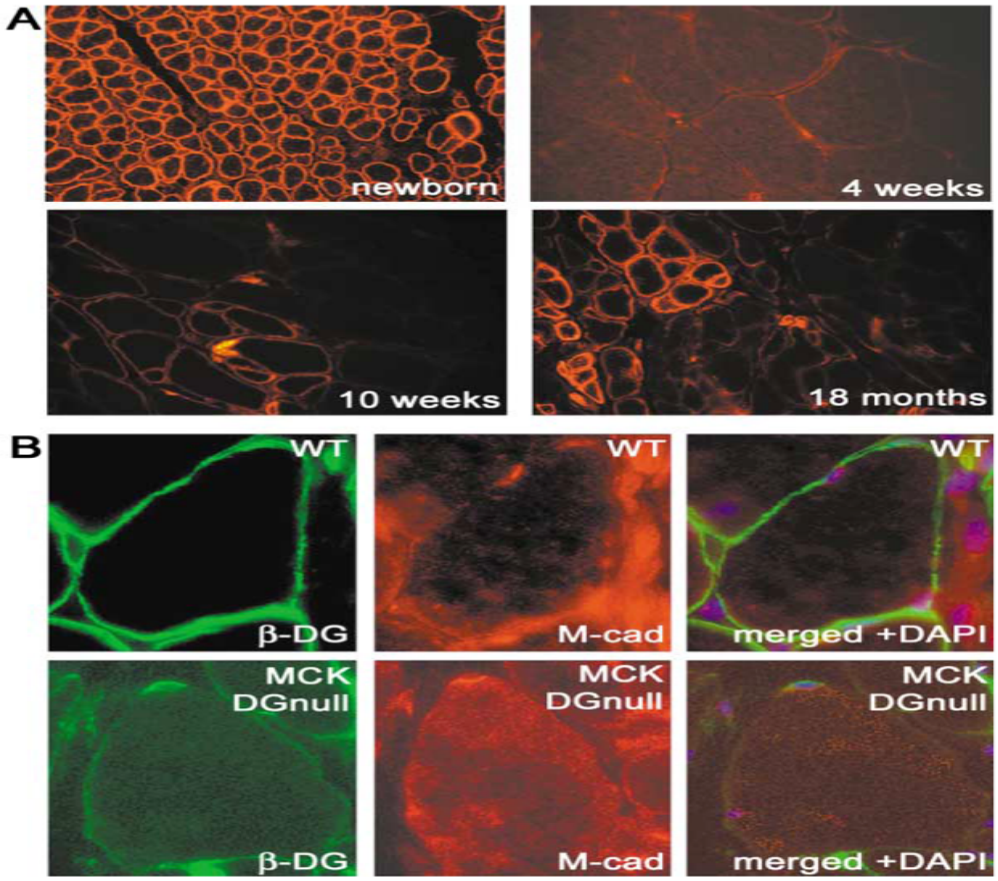

Figure 3. Dystroglycan Is Expressed in Satellite Cells

(A) Analysis of dystroglycan expression at various ages in *MCK-DG null* mice. Interestingly, dystroglycan is normally expressed in newborn skeletal muscle. In contrast, at 4 weeks of age, dystroglycan is nearly absent from the sarcolemma. Subsequently, *MCK-DG null* mice develop muscular dystrophy with ongoing cycles of necrosis and regeneration. After onset of the dystrophic process, clusters of dystroglycan-positive muscle fibers are observed in *MCK-DG null* mice between 10 weeks and 18 months of age (antibody AP 83 against β-dystroglycan).

(B) Expression of dystroglycan in satellite cells of wild-type and *MCK-DG null* mice. Double labeling with M-cadherin reveals enhanced membrane staining of the satellite cell toward the cytoplasm of the myofiber, whereas dystroglycan expression seems to be enhanced toward the basal lamina. The merged image including DAPI demonstrates the single nucleus of the satellite cell.

How do you treat CMD glycosylation disorders?

1. Overexpression of LARGE bypasses other genetic defects.
2. FKRP mutations for LGMD2I may not be loss of function. Protein is mislocalized but may still be functional.

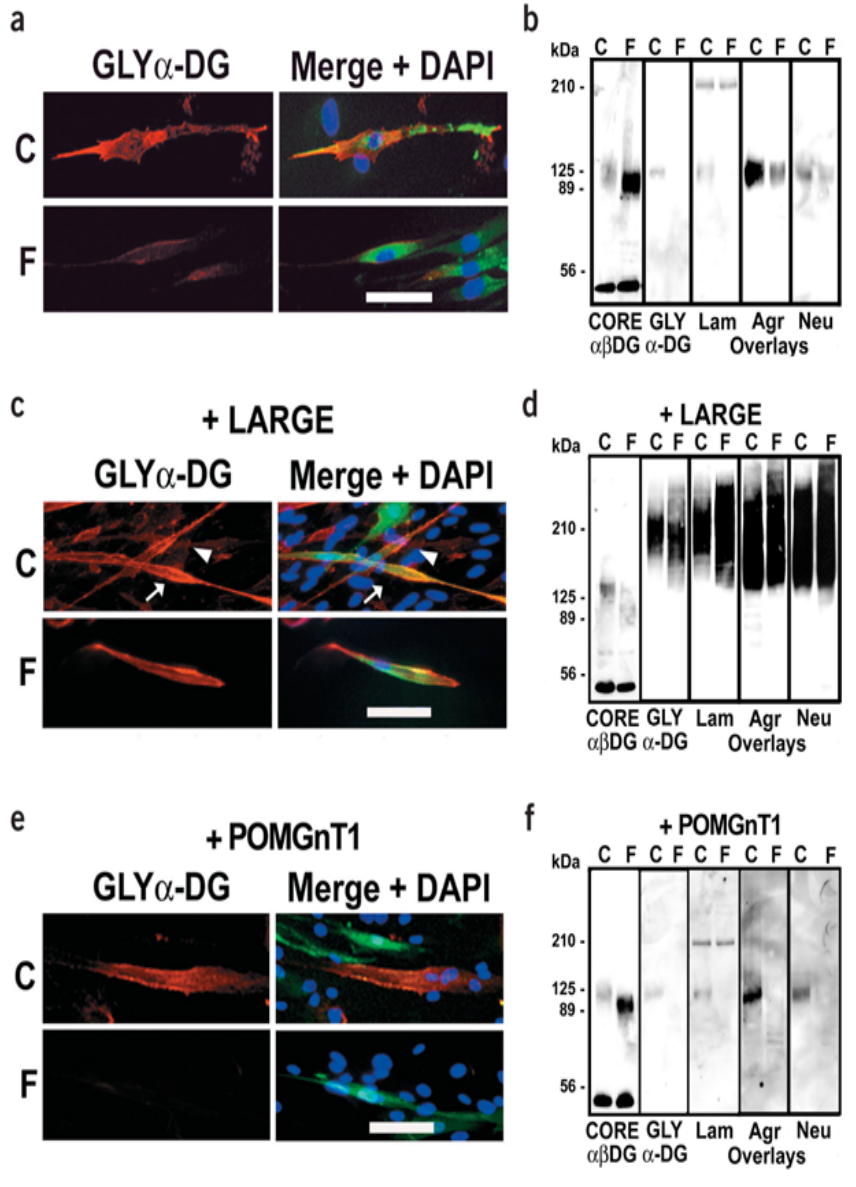

Figure 2 LARGE generates functional α-DG in FCMD myoblasts. (**a**–**f**) Analysis of untreated (**a**,**b**), or infected with Ad5-LARGE-eGFP (**c**,**d**) or Ad5-POMGnT1-eGFP (**e**,**f**) control (C) and FCMD (F) cultures. Immunofluorescence shows localization of desmin (**a**) or eGFP (**c**,**e**). Arrows indicate myotubes and arrowheads indicate myoblasts. Scale bars, 10 μm. WGA-enriched lysates of treated cultures were also analyzed by SDS-PAGE followed by immunoblot analysis with antibodies to DG core protein (CORE-αβDG) and glycosylated α-DG (**b**,**d**,**f**). Laminin (Lam), neurexin (Neu) and agrin (Agr) were used for ligand overlay assays. Bands at ~210 kDa in **b** and **f** are endogenous laminin. Data are representative of three individuals with FCMD.

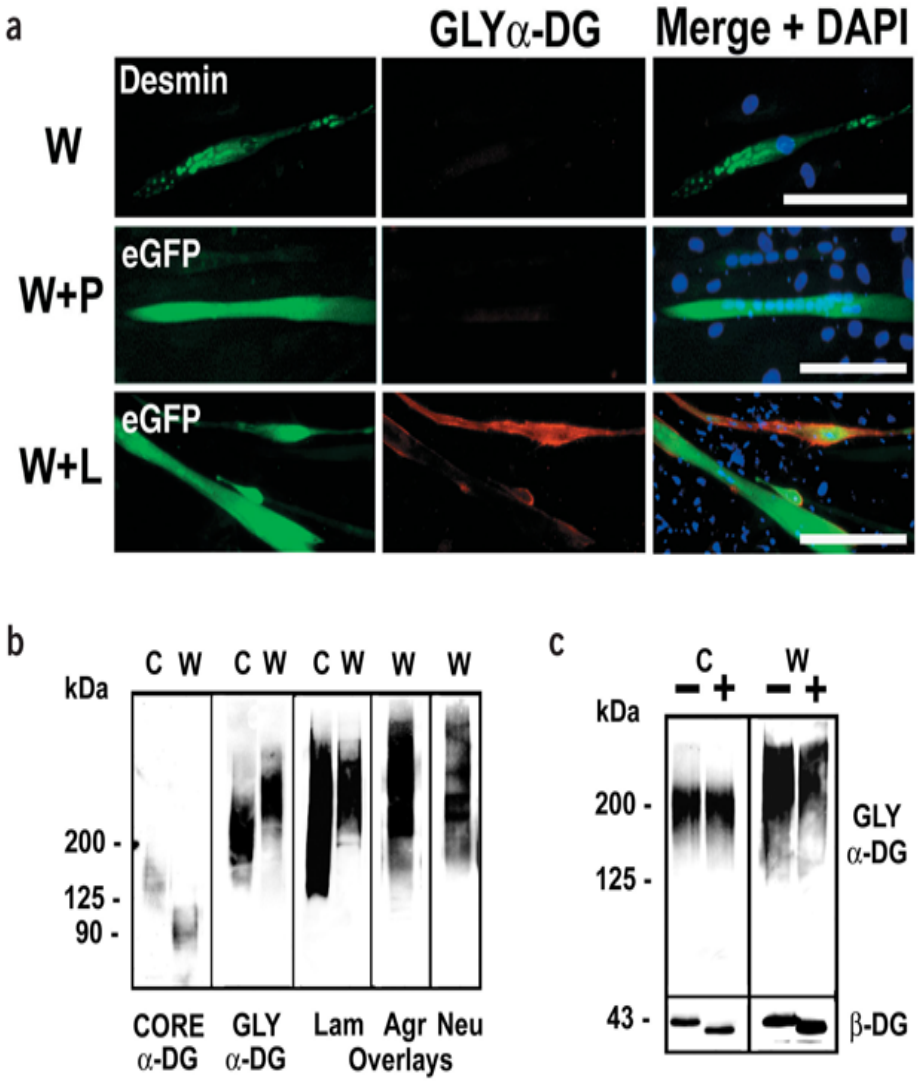

Figure 4 LARGE induces the synthesis of functional α-DG in WWS myoblasts and myotubes. (**a**) Expression of eGFP, desmin (green, upper row) and glycosylated α-DG (GLYα-DG), and nuclear labeling (DAPI, blue) in WWS myoblasts either untreated (W) or treated with Ad5-LARGE-eGFP (W+L) or Ad5-POMGnT1-eGFP (W+P). Scale bar, 20 μm. (**b**) Biochemical analysis of WGA-enriched fractions from control (C) and WWS myoblasts (W) treated with Ad5-LARGE-eGFP. Immunoblotting was done with antibodies to glycosylated α-DG and α-DG core protein (COREα-DG). Ligand overlay assays were done for laminin (Lam), agrin (Agr) and neurexin (Neu). (**c**) *N*-glycanase deglycosylation of WGA-enriched fractions from control (C) and WWS myoblasts (W) treated with Ad5-LARGE-eGFP. Immunoblotting was done with antibodies to β-DG and glycosylated α-DG. Untreated samples (–) are shown. Data are representative of four individuals with WWS.

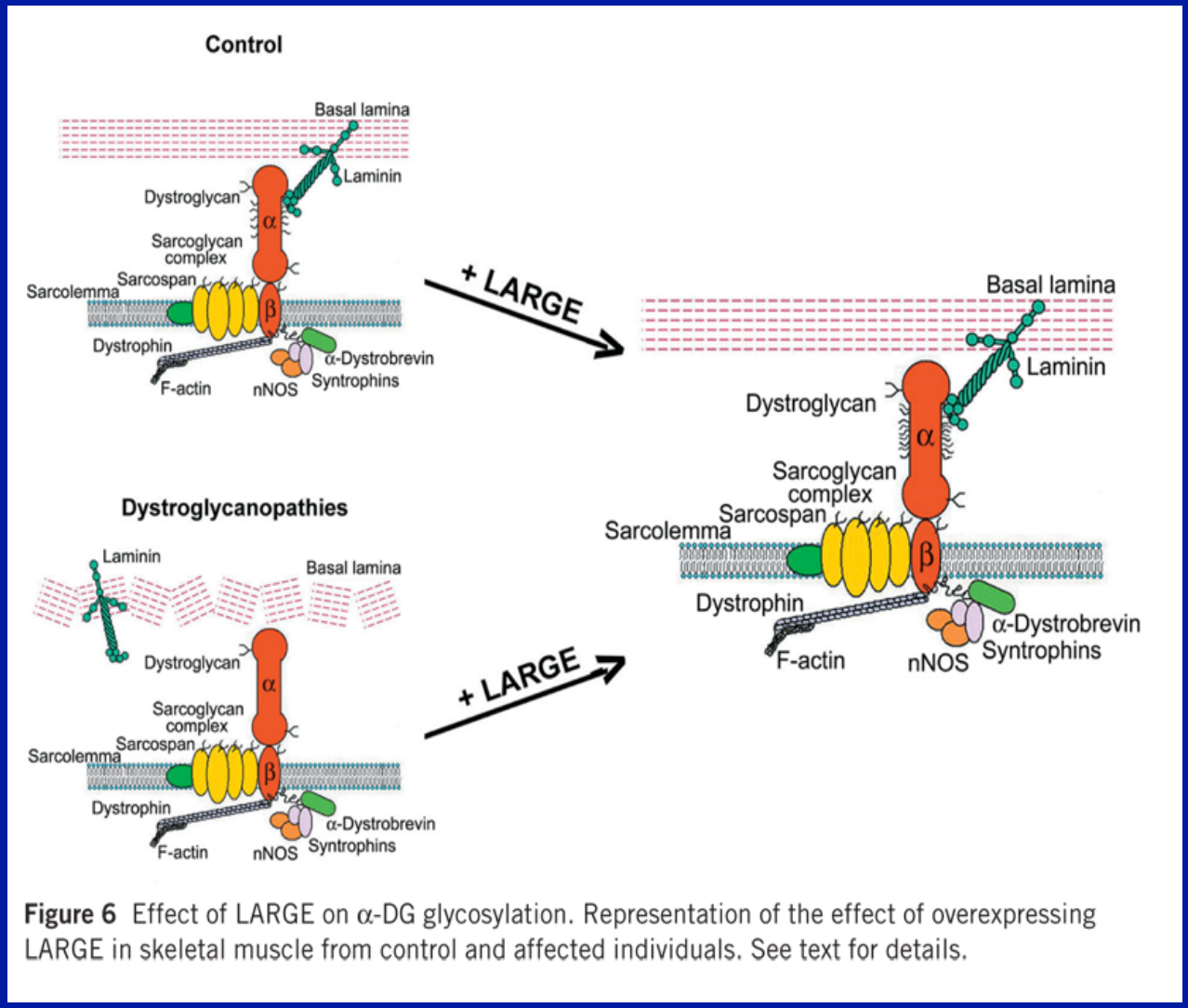

Figure 6 Effect of LARGE on α-DG glycosylation. Representation of the effect of overexpressing LARGE in skeletal muscle from control and affected individuals. See text for details.

LARGE Tg mice show increased glcosylation as per IIH6 blot, but lower specific force (Brockington et al. (2010) *PLOS one* 5, e14434)

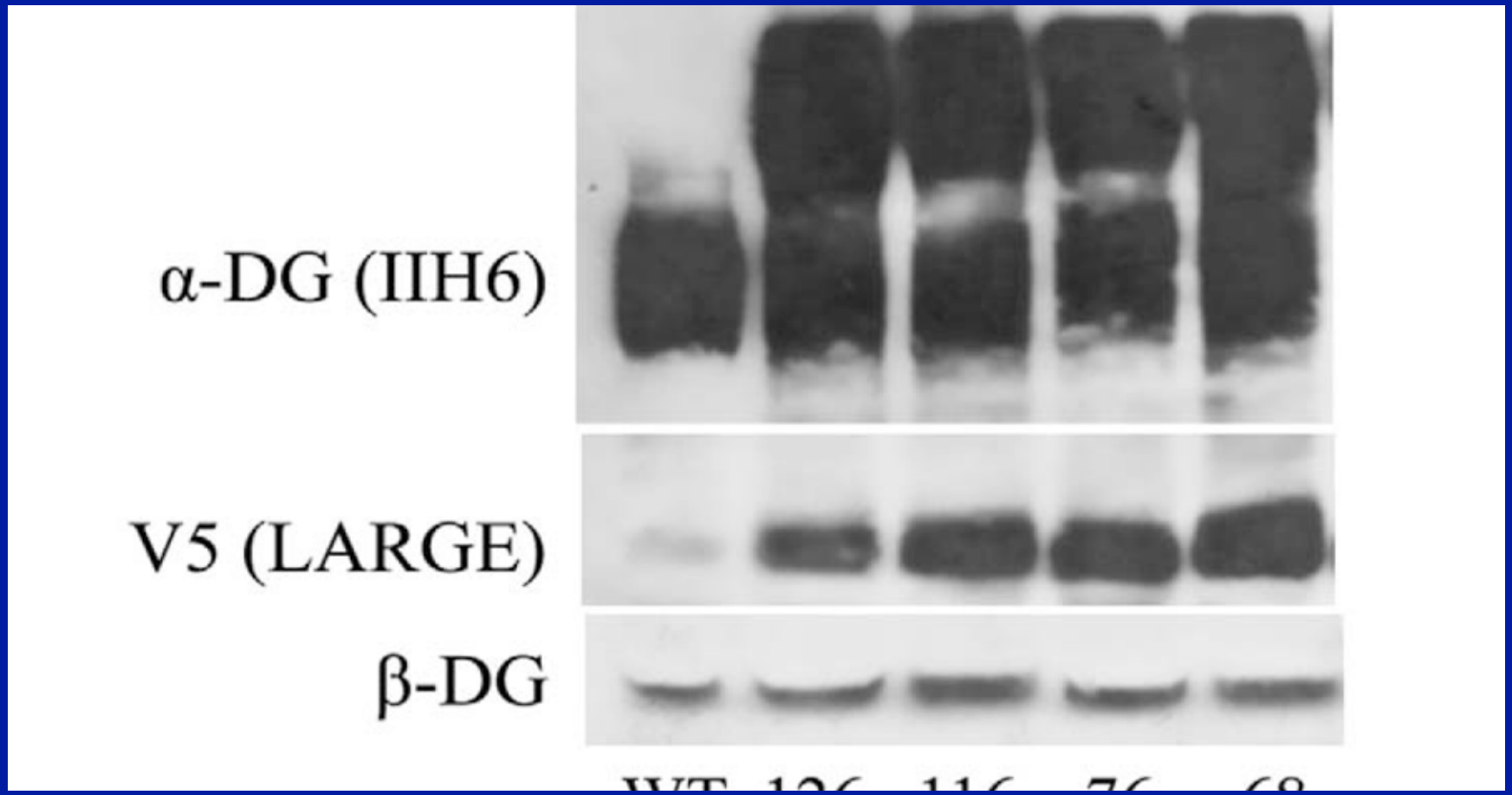

FKRP disease mutations mislocalize FKRP protein in cells

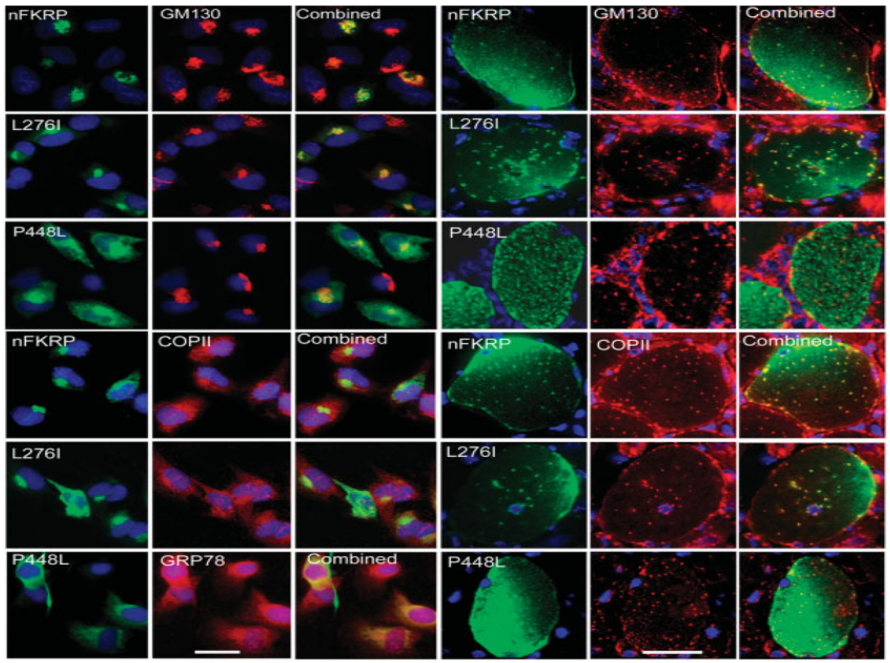

FIGURE 4. Colocalization of human normal and mutant FKRPs as recognized by antibodies specific to the Golgi apparatus (GM130), the ER-related transport vesicles (COPII protein), and ER (GRP78/BIP) in C2C12 cells (left three columns) and in the tibialis anterior muscles of *C57BL/10* mice (right three columns). The green fluorescence represents the FKRP expression and the red signals represent the staining with the antibody to GM130, COPII, and GRP78. Normal FKRP and L276I mutant FKRP localize at the Golgi apparatus in all or nearly all of the cells, respectively. The P448L protein is seen diffusely within the cytoplasm, although stronger signals were also observed in the Golgi area. Speckled signals can be identified in the fibers expressing nFKRP and mutant L276I proteins and are partially colocalized with the signals (red) identifying the GM130 and COPII proteins. No clear speckled patterns are observed in the fibers expressing the mutant P448L protein, although patches of stronger signal can be visualized. Nuclei are stained with DAPI (blue). Magnification: ×100. Scale bar, 50 μm.